Supporting Information

Hierarchically Porous Carbon Nanosheets from One-step Carbonization of Zinc Gluconate for High-Performance Supercapacitors

Zhiwei Tian [1,†], Zhangzhao Weng [2,†,*], Junlei Xiao [1], Feng Wang [1], Chunmei Zhang [3] and Shaohua Jiang [1,*]

The kinetics of the charge storage process can be evaluated ty the CV curves, where the total charge storage can be separated as the capacitive effects and diffusion-controlled charge storage, which can be expressed by the following eq (S1) and eq (S2), where the i is the peak current, v is the scan rate, a and b are the fitting parameters:

$$i_{total} = i_{cap} + i_{diff} = av^b \quad \text{(S1)}$$

$$\log i = \log a + b\log v \quad \text{(S2)}$$

The capacitance contributions from the surface capacitive effects and the diffusion-controlled intercalation process can be quantitatively distinguished by eq (S3) and eq (S4). Where k_1v and $k_2v^{1/2}$ are the capacitive effects and diffusion-controlled intercalation process contributions, respectively:

$$I(V) = k_1 v + k_2 v^{1/2} \quad \text{(S3)}$$

$$i(V)/v^{1/2} = k_1 v^{1/2} + k_2 \quad \text{(S4)}$$

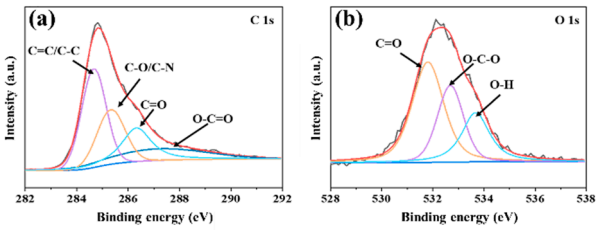

Figure S1 High-resolution of C 1s(a) and O 1s(b) of ZnPCN-1.

Table S1 Textural parameters of all samples.

Samples	S_{BET} (m^2 g^{-1}) [a]	V_t (cm^3 g^{-1}) [b]	D_P (nm) [c]	N content (at %)
ZnPCN-0.5	1135	0.47	3.32	2.95
ZnPCN-1	1162	0.49	3.33	4.57
ZnPCN-2	1146	0.48	3.38	4.40

[a] BET surface area.

[b] Total pore volume.

[c] Desorption average pore diameter by BET method.

Table S2 Comparison of ZnPCN-1 with the reported work.

Samples	Current density	Specific capacitance	Electrolyte	Ref.
ZnPCN-1	1 A g^{-1}	221 F g^{-1}	6 M KOH	This work
C9-250k-12	0.5 A g^{-1}	197 F g^{-1}	1 M Na_2SO_4	[1]
MA6	0.5 A g^{-1}	182 F g^{-1}	3 M KOH	[2]
SAK	2 mVs^{-1}	129 F g^{-1}	PVA/LiCl	[3]
SSP-900	1 A g^{-1}	199 F g^{-1}	3 M KOH	[4]
Gna-CA	1 A g^{-1}	140 F g^{-1}	1 M Na_2SO_4	[5]

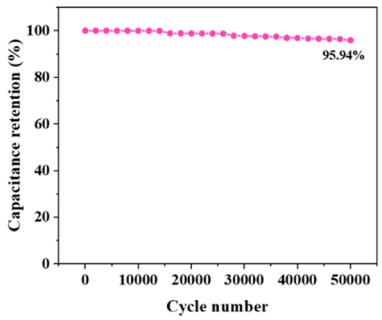

Figure S2 Cycling performance of ZnPCN-1 at a current density of 50 A g^{-1} in 6 M KOH.

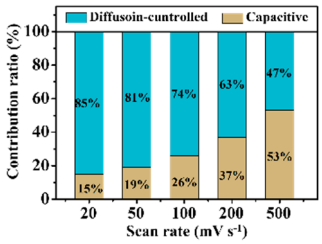

Figure S3 Capacitance contribution ratios of ZnPCN-1 at different sweep rates.

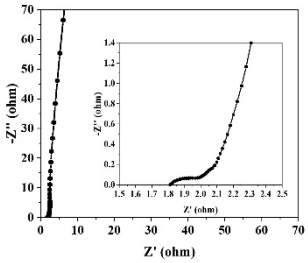

Figure S4 EIS plots of ZnPCN-1//ZnPCN-1 in 6 M KOH.

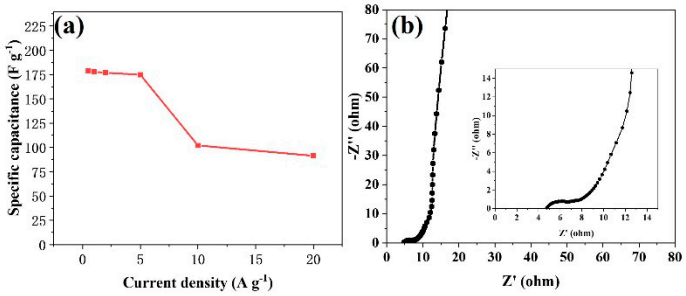

Figure S5 Rate performance (a), EIS plots (b) of ZnPCN-1//ZnPCN-1 in Et_4NBF_4.

Table S3 Comparison of ZnPCN-1//ZnPCN-1 with the reported work.

Samples	Energy density (Wh Kg^{-1})	Power density (W Kg^{-1})	Electrolyte	Ref.
ZnPCN-1//ZnPCN-1	17.2	499	6 M KOH	This work
ZnPCN-1//ZnPCN-1	153.4	1242	1 M Et_4NBF_4	This work
WC-E-100-48//WC-E-100-48	11.0	26.3	6 M KOH	[6]
WBMs-800//WBMs-800	9.4	227	6 M KOH	[7]
$Co(OH)_2$@CW//CW	6.5	236	2 M KOH	[8]
NiCo-P//CW	12.1	395	2 M KOH	[9]
N-M-O//Carbon	20.1	226	1 M Na_2SO_4	[10]
MnO_x/PANI//Carbon	37.0	800	H_2SO_4/PVA	[11]

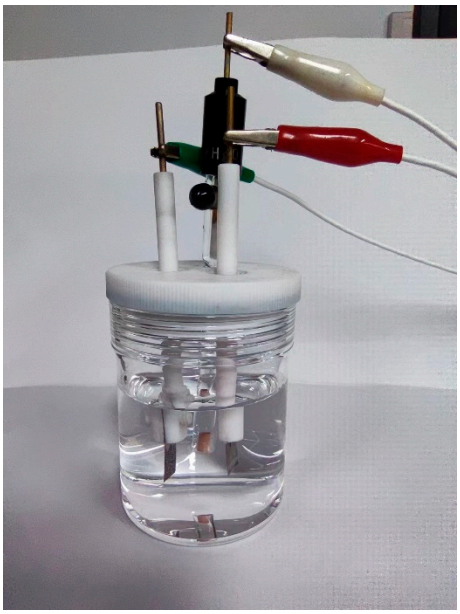

Figure S6 Photograph of the three-electrode system.

References

1. Zhang, W.; Li, W.; Li, S., Self-template activated carbons for aqueous supercapacitors. *Sustainable Materials and Technologies* **2023,** 36, e00582.
2. Khajonrit, J.; Sichumsaeng, T.; Kalawa, O.; Chaisit, S.; Chinnakorn, A.; Chanlek, N.; Maensiri, S., Mangosteen peel-derived activated carbon for supercapacitors. *Progress in Natural Science: Materials International* **2022,** 32, (5), 570-578.
3. Zhang, X.; Zhao, M.; Chen, Z.; Yan, T.; Li, J.; Ma, Y.; Ma, L., The application of biomass-based carbon materials in flexible all-solid supercapacitors. *Journal of Materials Science: Materials in Electronics* **2022,** 33, (19), 15422-15432.
4. Pandey, K.; Jeong, H. K., Coffee waste-derived porous carbon based flexible supercapacitors. *Chemical Physics Letters* **2022,** 809, 140173.
5. Fuertes, A. B.; Sevilla, M., Hierarchical Microporous/Mesoporous Carbon Nanosheets for High-Performance Supercapacitors. *ACS Applied Materials & Interfaces* **2015,** 7, (7), 4344-4353.
6. Wang, F.; Cheong, J. Y.; Lee, J.; Ahn, J.; Duan, G.; Chen, H.; Zhang, Q.; Kim, I. D.; Jiang, S., Pyrolysis of Enzymolysis-Treated Wood: Hierarchically Assembled Porous Carbon Electrode for Advanced Energy Storage Devices. *Advanced Functional Materials* **2021,** 31, (31), 2101077.
7. Ma, Y.; Yao, D.; Liang, H.; Yin, J.; Xia, Y.; Zuo, K.; Zeng, Y.-P., Ultra-thick wood biochar monoliths with hierarchically porous structure from cotton rose for electrochemical capacitor electrodes. *Electrochimica Acta* **2020,** 352, 136452.
8. Wang, Y.; Lin, X.; Liu, T.; Chen, H.; Chen, S.; Jiang, Z.; Liu, J.; Huang, J.; Liu, M., Wood-Derived Hierarchically Porous Electrodes for High-Performance All-Solid-State Supercapacitors. *Advanced Functional Materials* **2018,** 28, (52), 1806207.
9. Chen, Y.; Hou, H.; Liu, B.; Li, M.; Chen, L.; Chen, C.; Wang, S.; Li, Y.; Min, D., Wood-derived scaffolds decorating with nickel cobalt phosphate nanosheets and carbon nanotubes used as monolithic electrodes for assembling high-performance asymmetric supercapacitor. *Chemical Engineering Journal* **2023,** 454, 140453.
10. Xuan, H.; Xu, Y.; Liang, T.; Liang, X.; Xie, Z.; Han, P.; Du, Y., Molten Salt Synthesis of Na-Mn-O Composites as Electrode Materials for High-Performance Supercapacitors. *ChemElectroChem* **2019,** 6, (6), 1838-1845.
11. Ye, Q.; Luo, Y.; Cen, Q.; Dong, R.; Luo, T.; Xu, X.; Wang, F.; Li, B., In situ hybridization of polyaniline on Mn oxide for high-performance supercapacitor. *Journal of Energy Storage* **2021,** 36, 102330.